CHAPTER FIVE

Electron Tranport and Electrocatalytic Properties of MWCNT/Nickel Nanocomposite: Hydrazine and Diethylaminoethanethiol as Analytical Probes*

* The publication below resulted from part of the research work presented in this chapter and it is not referenced further in this thesis:

4. **Abolanle S. Adekunle**, Kenneth I. Ozoemena, *J. Electroanal. Chem.* 645 (2010) 41-49.

5.1 Comparative TEM, XRD and EDX spectra

Figures 5.1 (a) and (b) showed the comparative transmission electron microscopy (TEM) images of the pristine and acid treated MWCNTs. The pristine MWCNTs are cylindrical, long and capped at the edges (Figure 5.1a), but on harsh treatment in the acid medium, the tubes were cut to shorter length with cut edges (Figure 5.1b) which provided the platform for modification with the acidic functional groups.

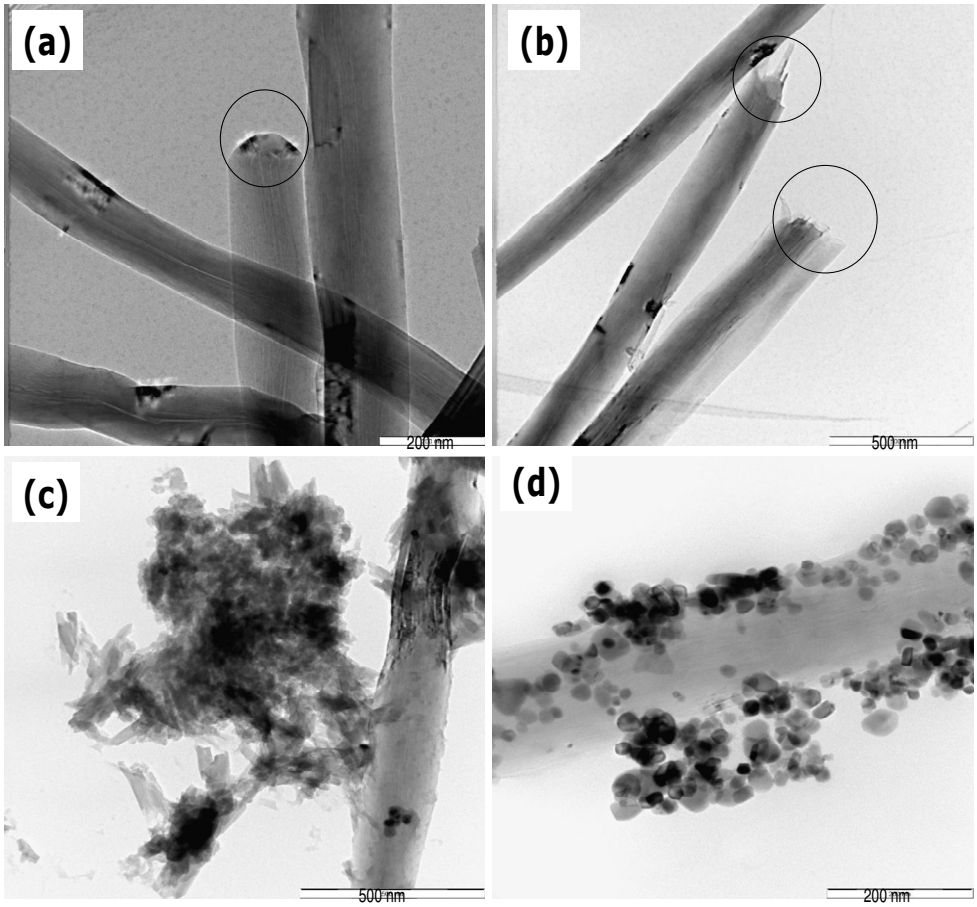

Figure 5.1: TEM images of (a) Pristine MWCNT (b) MWCNT-COOH (c) MWCNT-Ni and (d) MWCNT-NiO.

Typical TEM micrographs and size distributions for the nickel (c) and the nickel oxide (d) nanoparticles on MWCNT support are also represented in Figure 5.1 above. The Ni nanoparticles appear a little amorphous than their NiO counterparts that are very fine, crystalline mono-disperse nanoparticles. The NiO nanoparticle sizes are in the 25 – 50 nm range. The corresponding XRD spectra for the resultant particles are shown in Figure 5.2a. Three characteristic peaks for Ni (2θ = 43.4, 50.6 and 74.5), corresponding to Miller indices (111), (200) and (222) were observed [1]. The result agreed with that observed by Wu and Chen [1], which indicates that the resultant particles were pure face-centered cubic (fcc) nickel. On the other hand, it was difficult to obtain the Ni peak for the synthesised Ni nanoparticles (inset in Figure 5.2a) probably due to the amourphous nature of the particles. From Debye-Scherrer formula [2]:

$$d = \frac{K\lambda}{B\cos\theta} \tag{5.1}$$

where d is the average crystal size; K is a constant (0.89); λ is the wavelength (1.78901 nm) used; B is the full width at half maximum of the peak, θ is the Bragg's angle of the XRD peak, the crystal size of the NiO particles were estimated from the three peaks to be ~ 21.5 nm, which falls in the range shown by the TEM.

Figure 5.2b and c are the EDX profiles of the synthesised MWCNT-Ni and MWCNT-NiO, respectively. MWCNT-Ni (b) and the MWCNT-NiO (c) showed the presence of Ni peaks with very pronounced intensity corresponding to about 86% Ni implying that almost all the Ni^{2+} ions were successfully reduced to Ni nanoparticles. The occurrence of O

peak in (c) confirms the modification of the Ni to its NiO nanoparticles.

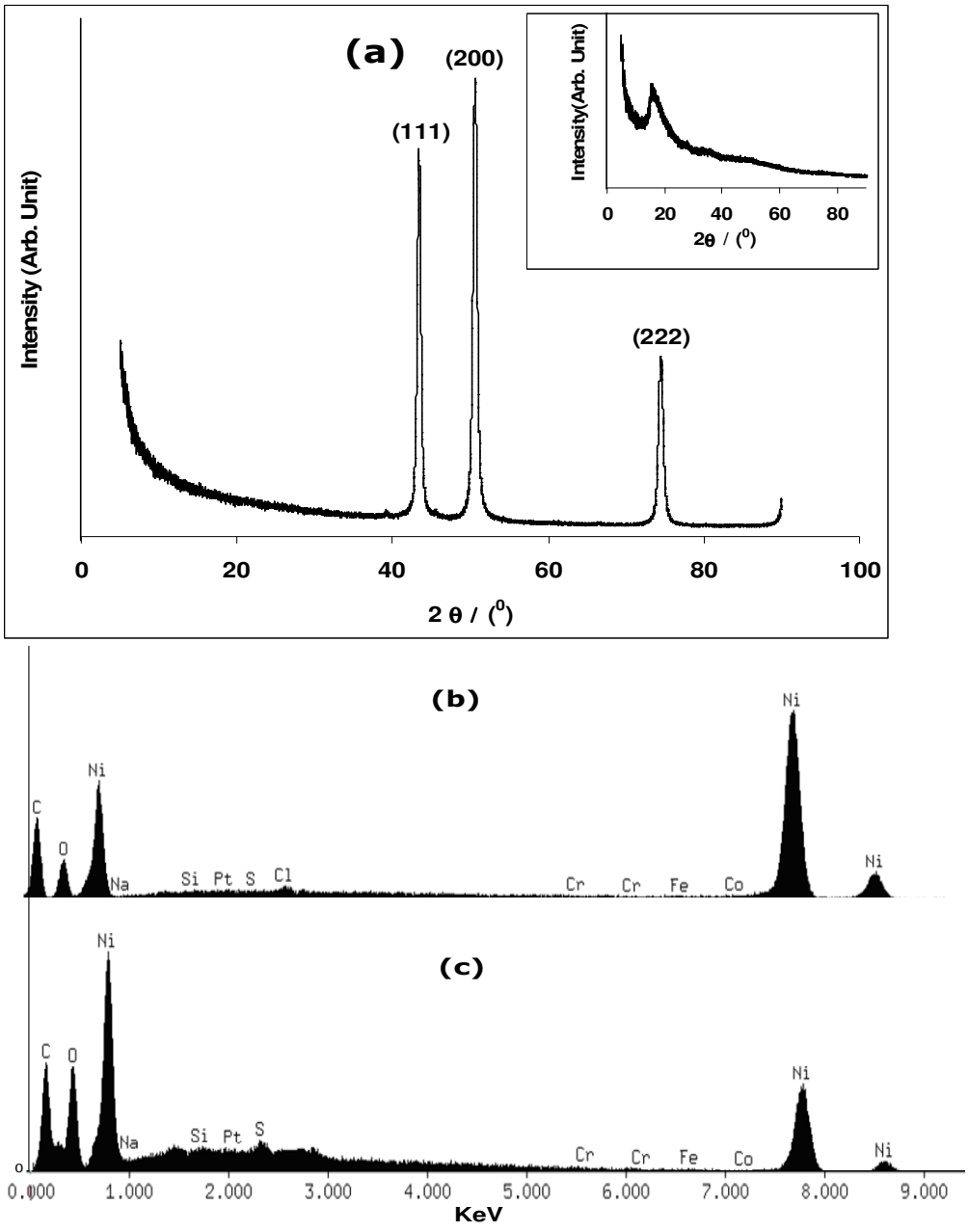

Figure 5.2: (a) XRD spectrum of NiO. Inset in (a) is the XRD spectrum of Ni. (b) and (c) represent the EDX spectra of MWCNT-Ni and MWCNT-NiO, respectively.

5.2 Comparative Electrochemical characterization

Figure 5.3 compares the cyclic voltammograms of the bare and modified EPPGEs in 0.1 M PBS (pH 7.0) (Figure 5.3a) and 5 mM $Fe(CN)_6]^{4-}/[Fe(CN)_6]^{3-}$ solution (Figure 5.3b). From Figure 5.3a, the bare EPPGE and EPPGE-MWCNT did not show any noticeable redox couple in the electrolyte employed in this work. On the contrary, all the nickel or nickel oxide based electrodes clearly showed the Ni^{2+}/Ni^{3+} redox process at formal or equilibrium potential ($E_{1/2}$) of about 0.35 V. All their peak-to-peak separation potential (ΔE_p) is ≥ 100 mV, greater than the theoretical 59.8 mV expected for a fast one-electron transport. Also, the ratios of the anodic to the cathodic peak current response (I_{pa} / I_{pc}) for these electrodes are approximately unity, indicative of reversible electrochemical process. Note that the EPPGE-MWCNT-Ni is characterised by higher current response compared to other electrodes investigated, about twice to that of the EPPGE-Ni, indicating that the enhancement of electrochemical performance arise from the synergy between the MWCNTs and the Ni nanoparticles.

The cyclic voltammetry in the solution of outer-sphere redox probe, $Fe(CN)_6]^{4-}/[Fe(CN)_6]^{3-}$, showed a pair of redox couples in the regions of 0 – 0.3 V (attributed to the $Fe(CN)_6]^{4-}/[Fe(CN)_6]^{3}$ redox process, with $E_{1/2} \approx 0.2$ V and $\Delta E_p \approx 0.17$) and in the 0.3 – 0.7 V region (attributed to the Ni^{2+}/Ni^{3+} redox process, with $E_{1/2} \approx 0.42$ V and $\Delta E_p \approx 0.12$). Like in the PBS solution, the MWCNT-Ni is associated with large current response. Note that in both electrolyte conditions, the voltammogramms of the Ni and NiO nanoparticles are slightly broad with wide ΔE_p.

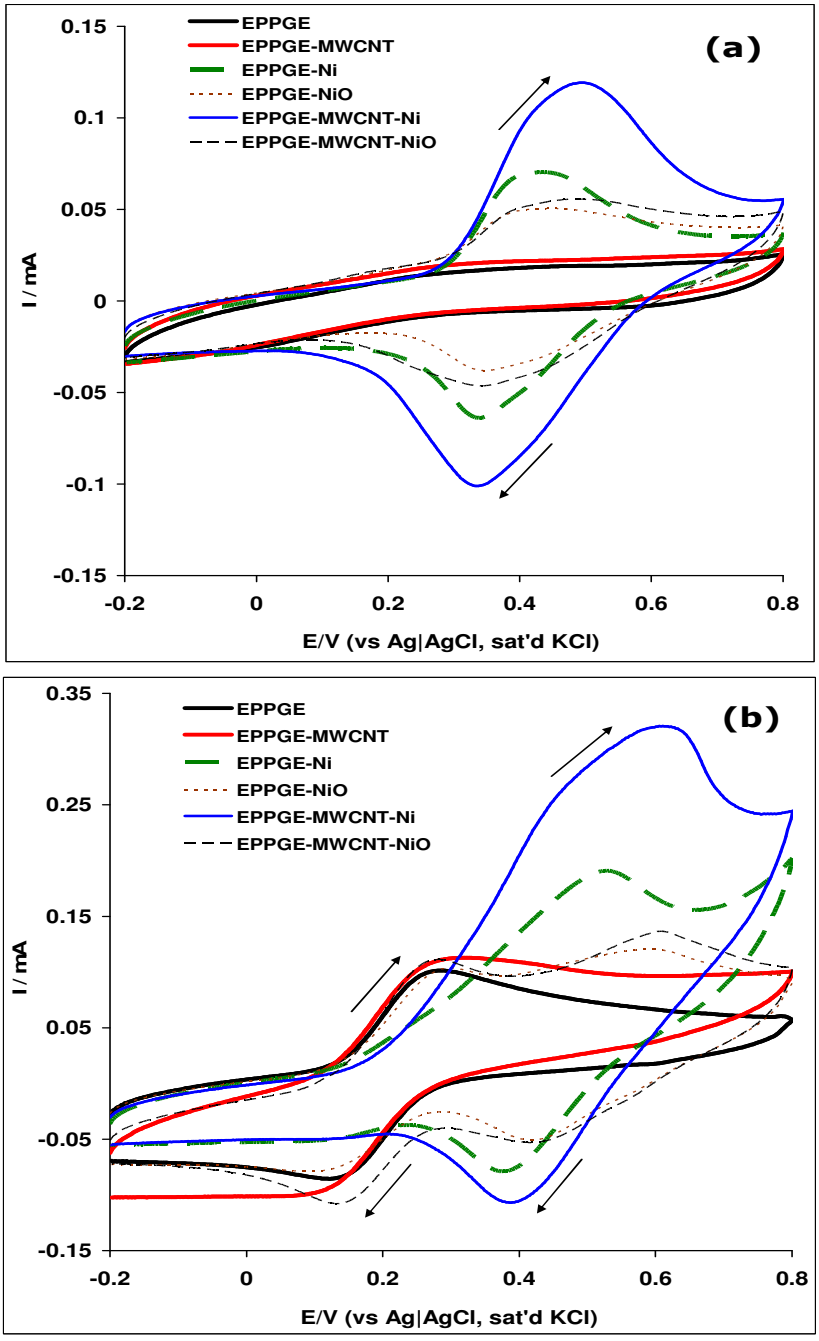

Figure 5.3: Comparative cyclic voltammetric evolutions of the electrodes in (a) 0.1 M PBS (pH 7.0), scan rate = 100 mVs^{-1}. (b) 5 mM $[Fe(CN)_6]^{4-}$ / $[Fe(CN)_6]^{3-}$ solution (in PBS pH 7.0). Scan rate = 50 mVs^{-1}.

This may be related to the different locations of these nanoparticles at the different environments of the MWCNTs leading to different formal potentials [3]. In a nutshell, these results clearly confirm the successful integration of Ni or NiO nanoparticles into the MWCNT support.

Considering that the redox process of the $Fe(CN)_6]^{4-}$ /$[Fe(CN)_6]^{3-}$ occurred at essentially the same $E_{1/2} \approx 0.2$ V and $\Delta E_p \approx$ 0.17 V for all the electrodes, it becomes somewhat difficult to unequivocally establish the rate of the electron transfer for any of the electrodes. Thus, EIS was employed (at biased potential of 0.2 V) to determine the extent to which each of the electrodes permit the electron transport between the redox probe and the underlying EPPGE. Figure 5.4 shows typical Nyquist plot, satisfactorily fitted (judged by the chi-square function of $\leq 10^{-4}$, and relative % errors, corroborated by the goodness of the fitting lines, Table 5.1) using the modified Randles equivalent circuit (inset in Figure 5.4). Ideally, R_s and Z_w values should not be affected by modification of the electrode surface, but in practice slight deviations may occur [4, 5], possibly due to the resistances induced by the modifying films to the solution. The slight increase in the R_s and Z_w values for the EPPGE-MWCNT and BPPGE-MWCNT-Ni is not fully understood at this time but may be related to the interaction of the modifying films with the electrolyte.

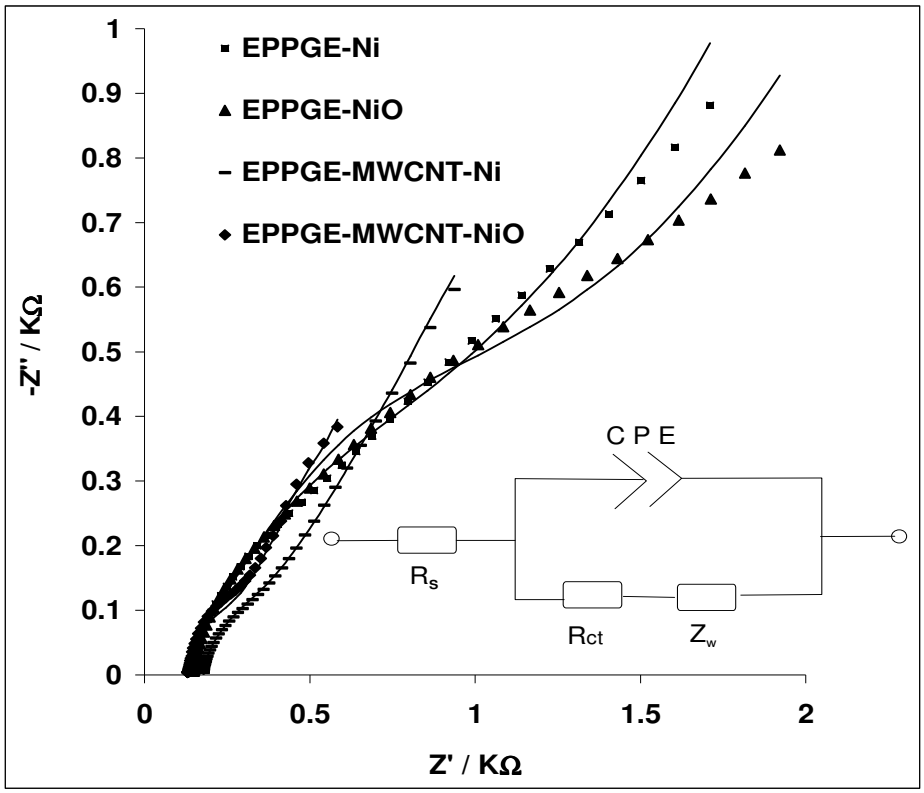

Figure 5.4: Typical Nyquist plots obtained for the electrodes in 5 mM $[Fe(CN)_6]^{4-}$ / $[Fe(CN)_6]^{3-}$ solution (PBS pH 7.0) at a fixed potential of 0.2 V (vs Ag|AgCl, sat'd KCl). Inset represents the circuit used in the fitting of the EIS data.

The values obtained from fitting the raw impedance spectra with this circuit (Table 5.1) indicates (from the values of the R_{ct}) that electron-transport is faster at the EPPGE-MWCNT-Ni and EPPGE-MWCNT-NiO electrodes compared to others. The slightly high R_{ct} of the former electrode may possibly be due to the more work done by this electrode in generating high current response compared to the latter. The n values are less than the ideal 1.0 expected from an ideal capacitive behaviour, thus suggesting pseudo-capacitive properties for these electrodes.

Table 5.1: Impedance data obtained for the bare EPPGE and the modified electrodes in 5 mM $Fe(CN)_6]^{4-}$ /$[Fe(CN)_6]^{3-}$ solution at 0.2 V (vs Ag|AgCl sat'd KCl).

Electrode	**Impedimetric Parameters**				
	R_s /Ω cm^2	CPE / μFcm^{-2}	n	R_{ct} /Ω cm^2	Z_W / mΩ cm^2
EPPGE	12.44 ±0.01	13.40 ±1.91	0.64 ±0.01	70.10 ±2.84	0.17 ±0.01
EPPGE-MWCNT	11.73 ±0.01	5.30 ±0.06	0.59 ±0.01	58.10 ±0.16	0.17 ±0.01
EPPGE-Ni	13.00 ±0.01	9.90 ±1.41	0.64 ±0.01	97.30 ±0.90	0.09 ±0.01
EPPGE-NiO	13.98 ±0.02	70.00 ±13.34	0.63 ±0.01	130.40 ±0.05	0.10 ±0.01
EPPGE-MWCNT-Ni	17.62 ±0.01	95.90 ±9.83	0.76 ±0.01	21.77 ±0.09	0.14 ±0.01
EPPGE-MWCNT-NiO	13.03 ±0.01	714.00 ±181.0	0.89 ±0.05	14.03 ±0.20	0.23 ±0.01

5.3 Comparative electrocatalytic properties: DEAET and Hydrazine as analytical probe.

Figure 5.5 presents the comparative current responses of the electrodes in 0.1 mM DEAET in PBS solution pH 9.4 (Figure 5.5a) and 1.0 mM hydrazine in 0.1 M Na_2SO_4 solution (Figure 5.5b). EPPGE-MWCNT-Ni demonstrated the best electrocatalytic properties with a less positive onset potential of about 0.2 V for DEAET (Figure 5.5a) and 0.3 V for the hydrazine (Figure 5b). Since EPPGE-MWCNT-Ni electrode gave the best result from the catalysis study, the effect of Ni nanoparticle loading on the electrocatalysis towards DEAET and hydrazine was investigated. From the cyclic voltammograms in Figure 5.6, the current responses (after background current subtraction) due to DEAET (Figure 5.6a) and hydrazine (Figure 5.6b) at different loadings of the Ni nanoparticles (2.5 to 10 mg) showed that a maximum current was reached at 7.5 mg and 2.5 mg of Ni nanoparticles for DEAET and hydrazine, respectively. The drop in current response after 7.5 mg Ni for DEAET or 2.5 mg Ni for hydrazine could be due to factors such as: (i) the transformation of the electrode surface to an insulator due to the high concentrations of the surface-confined nickel nanoparticles, which may be interpreted as a result of the increased electrical resistance and the resistance to mass transport through the film as the film thickness increases [6], and (ii) hydrazine is a strong reducing agent and can easily co-ordinate more and reduce the nickel nanoparticles as concentrations increases.

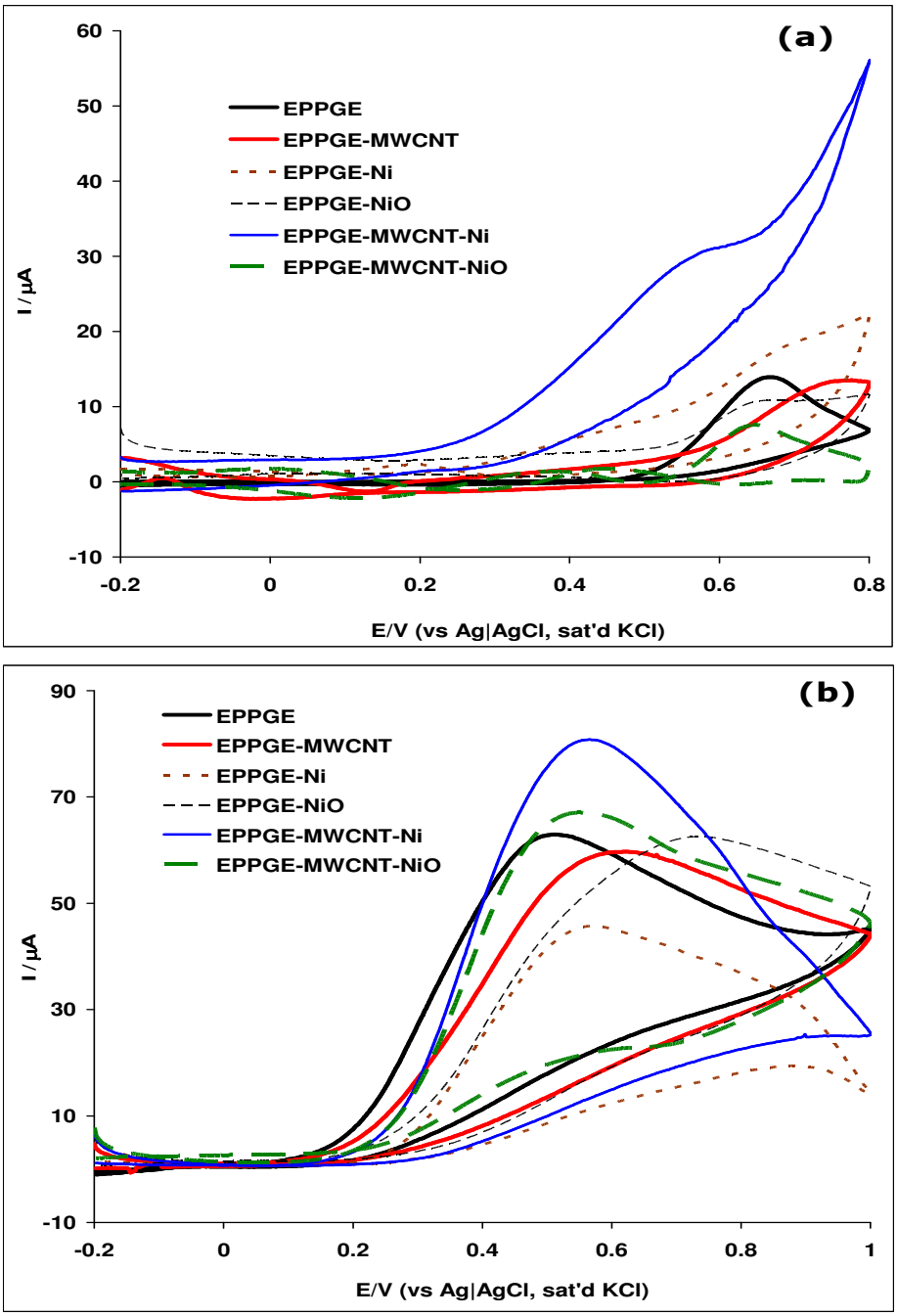

Figure 5.5: Comparative current response (after background current subtraction) of the electrodes in (a) 0.1 mM DEAET solution in pH 9.4 PBS and (b) 1.0 mM hydrazine solution in 0.1 M Na_2SO_4, scan rate = 25 mVs^{-1}.

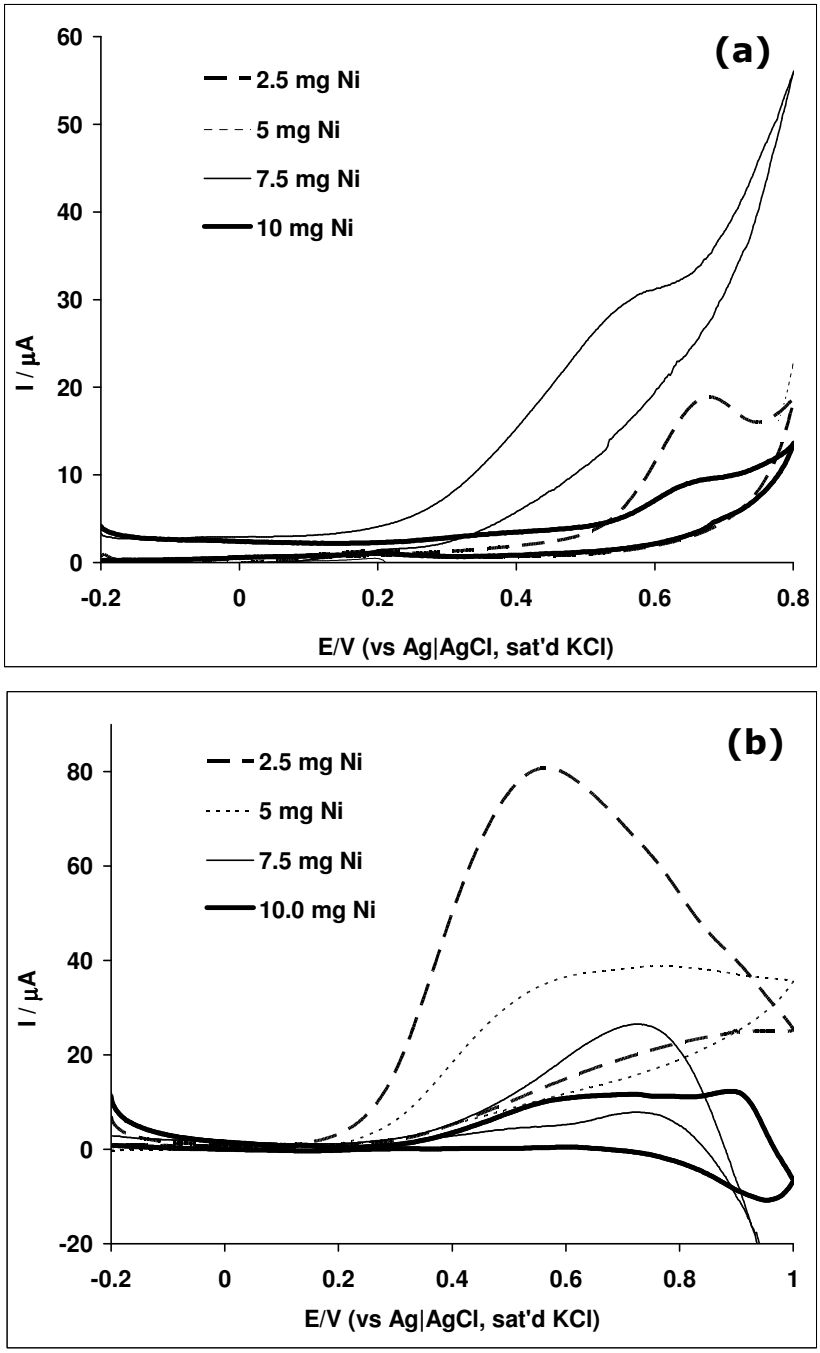

Figure 5.6 Comparative current response (after background current subtraction) for different Ni loading at the EPPGE-MWCNT-Ni electrode in (a) 0.1 mM DEAET solution in pH 9.4 PBS and (b)1.0 mM hydrazine solution in 0.1 M Na_2SO_4, scan rate = 25 mVs^{-1}.

To obtain some insights into the electrocatalytic oxidation, EIS was performed at the anodic oxidation potential, ~ 0.6 V of the analytes using the EPPGE-MWCNT-Ni electrode. Figure 5.7 shows the obtained Nyquist plot (a) and Bode plots (b) for these two analytes.

The raw impedance spectra were satisfactorily fitted with modified Randles equivalent circuit (Figure 5.7c), where L is an inductive element, R_{ad} is the resistance to adsorption, while the other elements are as already defined. R_{ad} and L are well known electrical elements associated with the adsorption of reaction intermediate(s) [7-9], clearly suggesting the involvement of the analytes intermediate products in the overall electrocatalytic oxidation process. The R_{ad} value is therefore interpreted here as the consequence of the adsorption of the intermediate(s) on the electrodes thereby creating an inductive effect on the electrode. For the DEAET, the EIS parameters are CPE (8.03 μFcm-^{2}), n (0.57), Z_w (2.60 μΩcm^2), L (0.37 mHcm^2) and R_{ad} (13.4 Ωcm^2). For the hydrazine, the parameters were CPE (1.32 μFcm-^{2}), n (0.46), Zw (2.87 μΩcm^2), L (0.23 mHcm^2) and R_{ad} (9.75 Ωcm^2). The presence of the Z_w in the circuit, coupled with the n values being close to the ideal Warburg diffusive value of 0.5, is indicative of some diffusion processes for these two analytes at this MWCNT-Ni electrode. Indeed, the occurrence of both L and Z_w (and n values) suggests both adsorption and diffusion-controlled reactions.

From the Bode plots (-phase angle vs log f), two phases' relaxation processes were observed at the low frequency (-0.6 Hz for DEAET) and high frequency (1.1 Hz for DEAET and 1.3 Hz for hydrazine) regions, an indication of a complex electrochemical process occurring at the electrode|electrolyte interface during the electrooxidation of the DEAET and hydrazine.

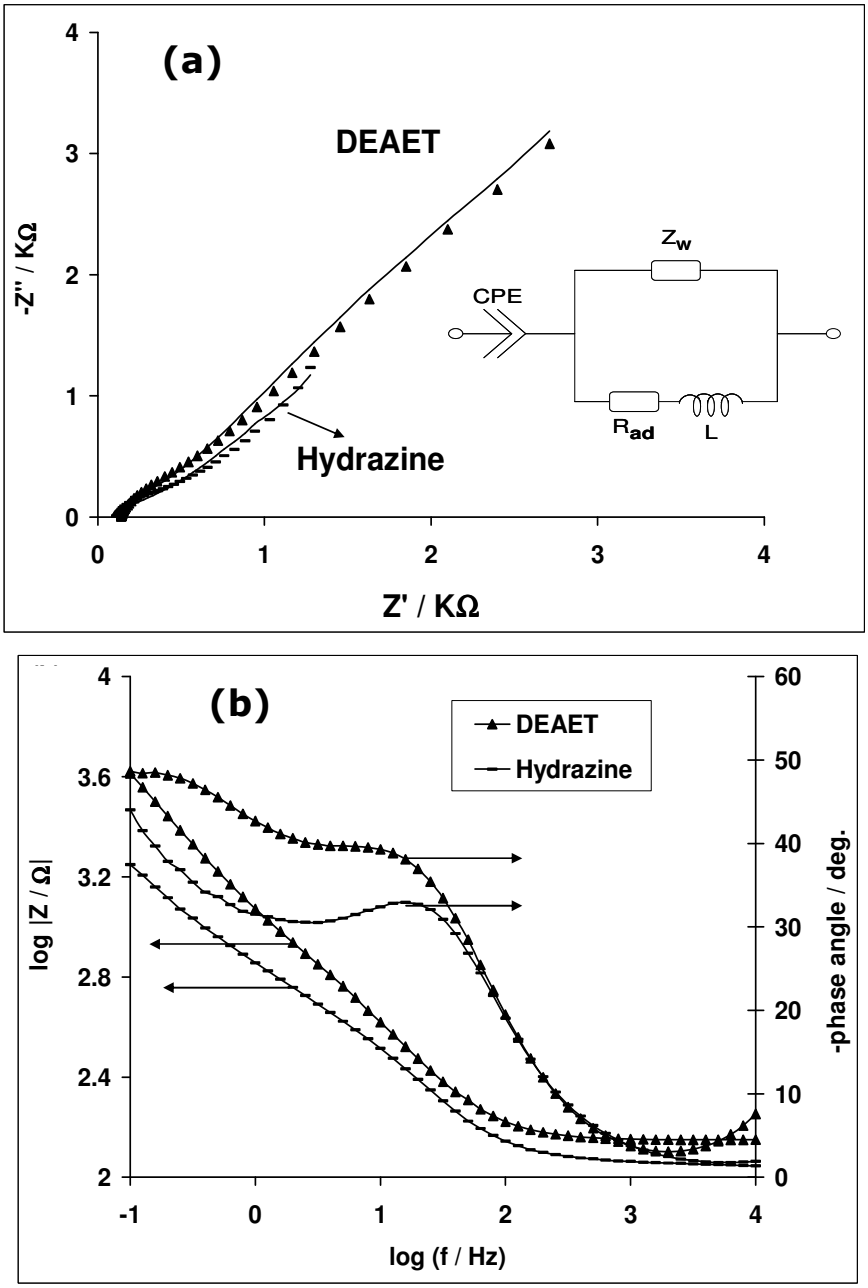

Figure 5.7: (a) Typical Nyquist plots obtained for EPPGE-MWCNT-Ni in 0.1 mM DEAET solution in PBS 9.4 and 1.0 mM hydrazine in 0.1 M Na_2SO_4 solution respectively (at fixed potential 0.6 V vs Ag|AgCl, sat'd KCl). (b) Represents the Bode plots obtained for the EPPGE-MWCNT-Ni, showing the plots of -phase angle / deg. vs log (f / Hz)) and the plot of log |Z/Ω| vs log (f/Hz) for both DEAET and hydrazine.

The complex process identified for DEAET from this study may also explain the two oxidation peaks noticed during the electroxidation of the analyte demonstrated by the voltammograms during the scan rate study discussed below. From the other Bode plots (log |Z| vs log f), the slope of the mid-frequency region (-0.54, R^2 = 0.9989) is indicative of pseudocapacitive behaviour, while the slope at the high frequency region (-0.41, R^2 = 0.9927) is indicative of strong resistance.

5.4 Effect of varying scan rates

The affect of scan rate (ν) using cyclic voltammetry at constant concentration of DEAET (0.1 mM) and hydrazine (1.0 mM) in the same electrolyte conditions as described already using the EPPGE-MWCNT-Ni was investigated. A gradual increase in current height with a slight shift in potential was observed with increase in scan rate (Figure 5.8a for DEAET and figure 5.8b for hydrazine) at scan rate ranging from 25 to 1400 mVs^{-1}. The hydrazine oxidation peak at around 0.6 V disappeared after 200 mVs^{-1}. Interestingly, the oxidation of DEAET (Figure 5.8a) is characterised by the occurrence of two oxidation peaks at about 0.6 and 1.0 V. This study represents the first time such two peaks have been observed for DEAET electro-oxidation on any electrode. DEAET, just like any other sulfhydryl analytes, contains functional groups HS and NH_2 which exist in different ionic states under different pH conditions and are thus responsible for the two anodic peaks. This interpretation is in agreement with a similar observation during the electrocatalytic detection of cysteine, a well known sulfhydryl [10].

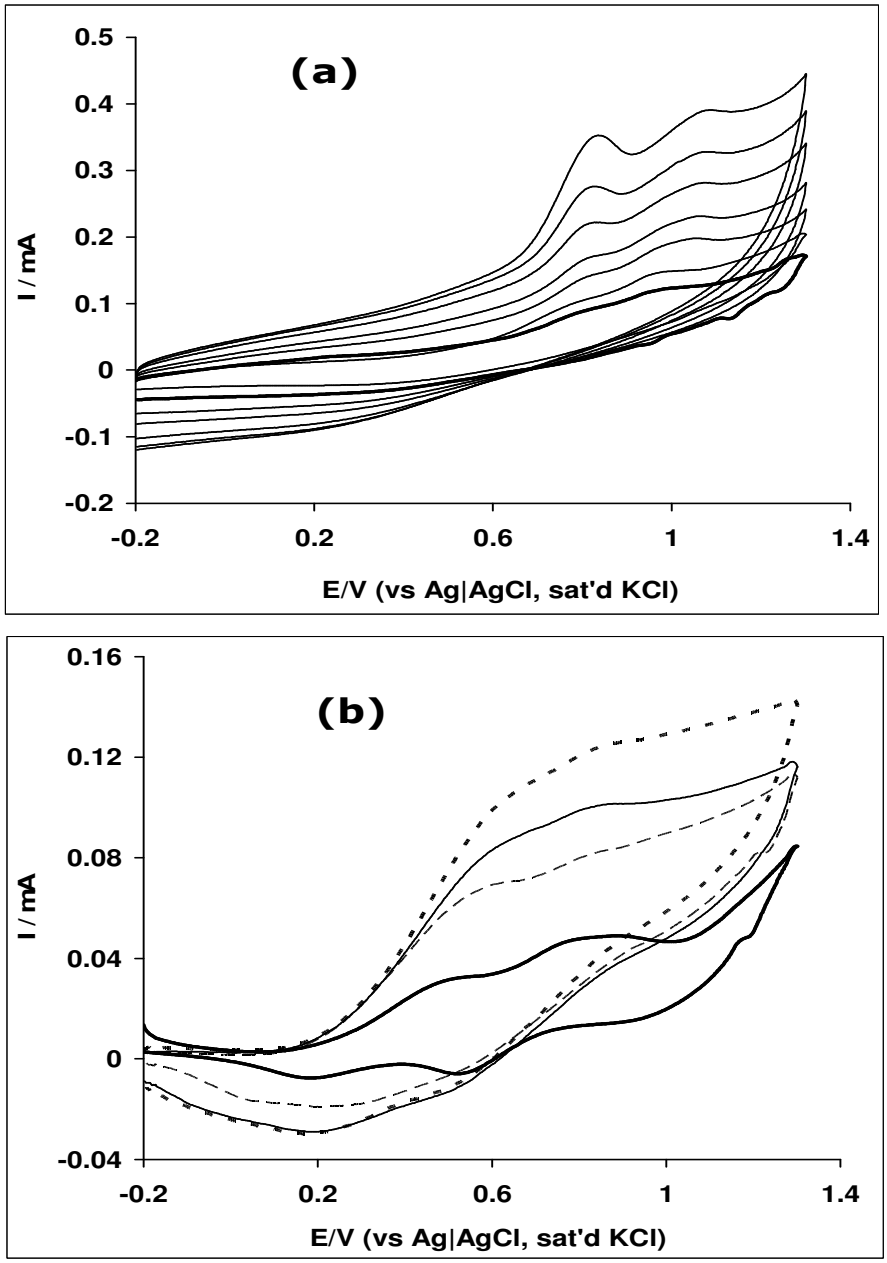

Figure 5.8: Cyclic voltammetric evolutions at the EPPGE-MWCNT-Ni for (a) 0.1 mM DEAET in 0.1 M pH 9.4 PBS (at 25, 75, 400, 600, 950, 1200 and 1400 mVs^{-1}, inner to outer), and (b) 1.0 mM Hydrazine in 0.1 M Na_2SO_4 solution after background subtraction (at 25, 75, 150 and 200 mVs^{-1}, inner to outer).

The two anodic peaks for DEAET oxidation at pH 9.4 were attributed to the oxidation of the two ionic forms of DEAET represented below:

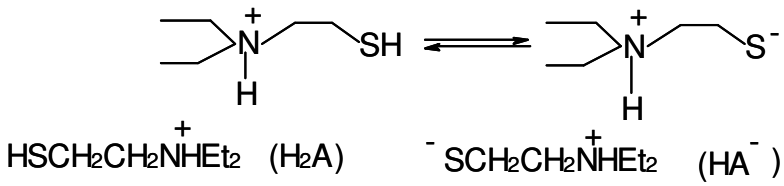

(5.2)

These two states are possible since in a less basic medium, the pKa of $HSCH_2CH_2N^+HEt_2$ is 8.3 at 25 ^{0}C [11], which is less than the pH of the medium and therefore could easily be deprotonated at pH 9.4 to give $^-SCH_2CH_2N^+HEt_2$. From the Randles-Sevčik theory for an anodic oxidation process [12], the plot of the peak current (I_p) against the square root of scan rate ($\nu^{1/2}$) gave a linear relationship (R^2 = 0.9925) for DEAET oxidation with approximately zero intercept, confirming a diffusion-controlled process. However, at higher scan rate (> 500 mVs^{-1}), plot of the peak current (I_p) against the square root of scan rate ($\nu^{1/2}$) (not shown) gave a straight line (R^2 = 0.9901) with a negative intercept suggesting that at higher scan rates the reaction is not totally diffusion-controlled. The result of the scan rate study (Figure 5.8b) for hydrazine electro-oxidation indicates adsorption of oxidation product(s) or fouling effect, evidenced by the disappearance of the hydrazine oxidation peak at around 0.5 V and that of the complex oxidation intermediate products at around 0.9 V after 200 mVs^{-1}, which may be related to the reductive activity of hydrazine solution towards nickel ions as reported by Bettahar et al. [13], thereby impeding the catalytic activities of the Ni nanoparticles. In addition, for both DEAET and hydrazine, the current function plot

showed that $I_p/\nu^{1/2}$ decreased as the scan rates increased, characteristic for coupled electrochemical and chemical reaction (EC_{cat}) mechanism.

Using Tafel equation (Equation 5.3) for a totally irreversible diffusion-controlled process [14], the linear relationship between the peaks potential E_p and the logν (not shown) confirms the chemical irreversibility of DEAET and hydrazine electrocatalytic oxidation processes.

$$E_p = \frac{b}{2}\log \nu \tag{5.3}$$

$$b = \frac{2.303RT}{\alpha n_\alpha F} \tag{5.4}$$

where R, T, α and n_α have their usual meanings. The plots of peak potential (E_p) against logarithm of scan rate (log ν) (not shown) gave a straight lines with Tafel slopes of approximately 262 and 406 mV dec^{-1} for the DEAET and hydrazine, respectively. These values are higher that the theoretical 118 mV dec^{-1} for a one-electron process involved in the rate-determining step. Such high Tafel values (leading to small α values, < 0.5) are the consequence of adsorption of reactants or intermediates on the electrode surfaces and/or reactions occurring within a porous electrode structure [15]. The Tafel slope is comparable with the values obtained using electrodeposited of Ni nanoparticles onto SWCNT.

5.6 Electroanalysis of DEAET and Hydrazine

Chronoamperometric (CA) and adsorptive linear sweep voltammetric (AdLSV) experiments were carried out for the two analytes. Figure 5.9 exemplifies typical CA (Figure 5.9a) and LSV

(Figure 5.9b) obtained for the hydrazine. The CA and LSV for the DEAET gave similar curves. The chronoamperograms were obtained by adding different aliquots of the analyte solution to their respective electrolyte solution. Each AdLSV curve was obtained after gently stirring the analyte for ~15 min in the presence of the electrode. From the CA curves, the catalytic rate constant (*k*) for each of the analyte was estimated using Equation 5.5 [12]:

$$\frac{I_{cat}}{I_L} = \pi^{1/2}\left(kC_o t\right)^{1/2} \qquad (5.5)$$

where all symbols have their usual meaning. From the plot of I_{cat}/I_L vs $t^{1/2}$ (not shown) the *k* value for the EPPGE-MWCNT-Ni in the solutions containing DEAET and hydrazine are ~ (5.9±0.50) x 10^9 and (7.7±0.66) x 10^8 $cm^3mol^{-1}s^{-1}$, respectively. The value of 5.9 x 10^9 $cm^3mol^{-1}s^{-1}$ is approximately three orders of magnitude greater than the 1123.59 $M^{-1}s^{-1}$ (i.e., 1.124 x 10^6 $cm^3mol^{-1}s^{-1}$) reported for DEAET electrocatalytic oxidation using basal pyrolytic graphite modified with SWCNT and cobalt(II)tetra-aminophthalocyanine (BPPGE-SWCNT-CoTAPc [16]). On the other hand, the 7.7 x 10^8 $cm^3mol^{-1}s^{-1}$ obtained for hydrazine is greater compared with 4.1 x 10^7 $cm^3mol^{-1}s^{-1}$ [17] reported for the analyte on gold-polypyrrole composite matrix modified glassy carbon electrode (Au/PPy/GCE), 2 x 10^7 $cm^3mol^{-1}s^{-1}$ for *o*-aminophenol modified glassy carbon electrode [18].

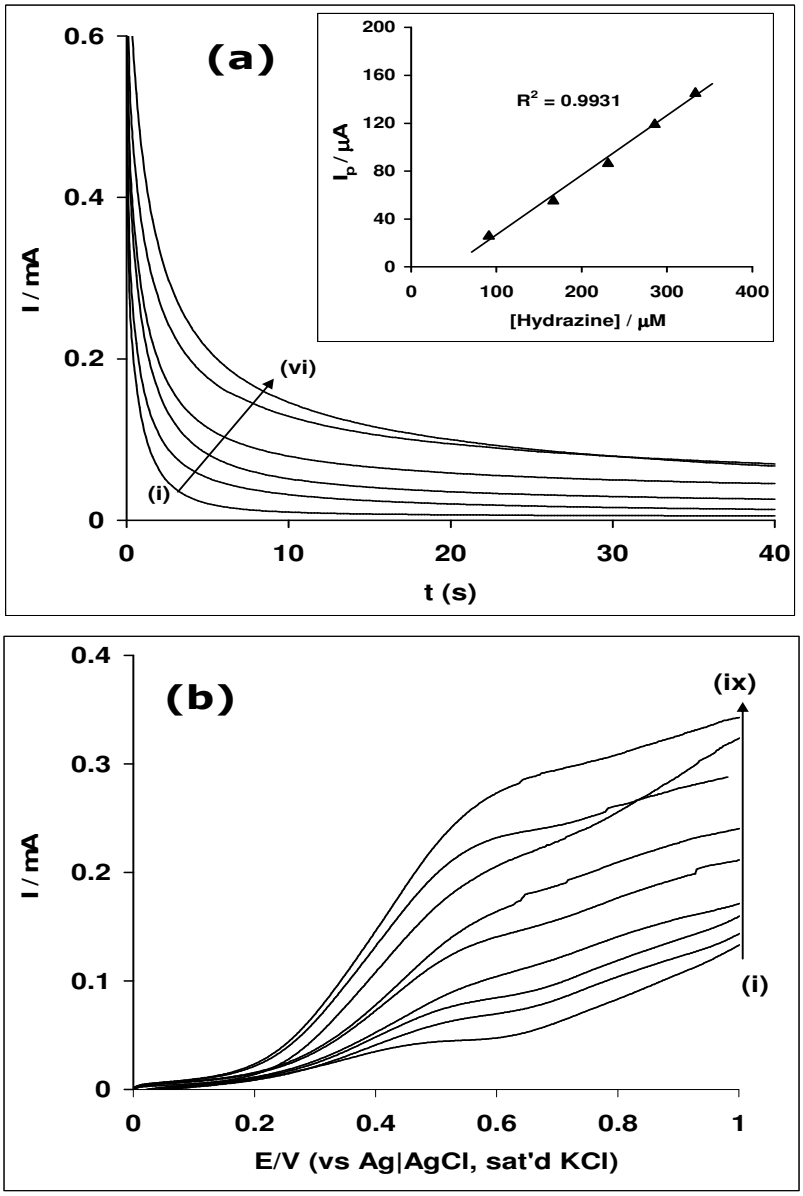

Figure 5.9: (a) Typical chronoamperograms obtained for the EPPGE-MWCNT-Ni in 0.1 M Na_2SO_4 solution containing different concentrations of hydrazine (0.0, 91, 167, 231, 286, and 333 µM, (i to vi)). Inset represents the plot of current response vs hydrazine concentration. (b) Typical linear sweep voltammograms obtained for the EPPGE-MWCNT-Ni in 0.1 M Na_2SO_4 solution containing different concentrations of hydrazine (0.0, 91, 130, 167, 231, 286, 333, 355, and 375 µM (i to ix)).

It is also greater than 6.26 x 10^6 $cm^3mol^{-1}s^{-1}$ for curcumin multi-walled nanotubes modified glassy carbon electrode [19], but about four orders of magnitude greater than reported (2.2x10^4 $cm^3mol^{-1}s^{-1}$) for electrodeposited Ni on SWCNTs. These results clearly indicate excellent catalysis for the chemically-synthesized Ni nanoparticles on MWCNTs towards these two analytes. Similarly, the plot of I_p versus [DEAET] gave the sensitivity values which are 13.6±0.33 $AM^{-1}cm^{-2}$ for DEAET and 3.33±0.13 $AM^{-1}cm^{-2}$ for hydrazine. The 3.33 $AM^{-1}cm^{-2}$ for for the electrode in hydrazine is greater compared to the 1.117 $AM^{-1}cm^{-2}$ reported for nanoporous gold particles modified platinum electrode [20]. The limit of detection was obtained using [21]:

$$LoD = 3.3\frac{\delta}{m} \tag{5.6}$$

The obtained LoDs are 0.87±0.07 and 0.29±0.02 μM for DEAET and hydrazine, respectively. The LoD value obtained in this study for DEAET is about 9 times lower than 8.0 μM obtained for screen-printed electrode modified with MWCNTs integrated with organophosphorus hydrolase [22]; ~3.5 times lower than the 3.0 μM reported at BPPGE-SWCNT-CoTAPc [16], and 3.0 μM reported for glassy carbon electrode modified with polypyrrole and pyrroloquinoline [23], ~ 4.6 times lower than 4.0 μM reported for BPPGE-Ni powder [4], and about 3 times lower than 2.5 μM for EPPGE-SWCNT-Ni (obtained by adsorption stripping voltammetry). The LoD value obtained for hydrazine (0.29 μM) is ~ 18 times lower compared to 5.3 μM detection obtained for EPPGE-SWCNT-Ni by electrodeposition. The enhanced sensitivity of the electrode used in this study and its very good limit of detection could be due to the

synergistic behaviour between the MWCNTs and the catalytic nickel nanoparticles, possibly affected by the method of electrode preparation adopted in this work. Table 5.2 compares the analytical data obtained in this work with literature [4,16,19,22,26,24-27].

Further probe into the adsorptive properties of hydrazine and DEAET was obtained from the AdLSV data. The voltammograms were analysed using the Langmuir adsorption isotherm theory [28]:

$$\frac{C}{I_{cat}} = \frac{1}{\beta I_{\max}} + \frac{C}{I_{\max}} \qquad (5.7)$$

where C, I_{cat} and I_{max} are already defined (section 1.7). β is the adsorption equilibrium constant, and is related to the electrochemical Gibbs free energy change (ΔG^o) as:

$$\Delta G^o = RT \ln \beta \qquad (5.8)$$

Each plot of the ratio of C/I_{cat} vs C gave straight line (not shown), suggesting an adsorption-controlled process. From the slopes and the intercepts of the curve obtained, the β value of each analyte was obtained, and then used to estimate the ΔG^o value. The ΔG^o values were −17.21 and −18.14 kJmol^{-1} for hydrazine and DEAET, respectively. There is no report to compare the ΔG^o value for hydrazine with at the moment. However, the ΔG^o obtained for DEAET in this study is lower than the value of −45.8 kJmol^{-1} on the EPPGE-SWCNT-Ni platform. The result further confirms the less adsorptive behaviour of the chemically-synthesized Ni nanoparticles on the MWCNT platform used in this study over the electrodeposited Ni nanoparticles on SWCNT platform.

Table 5.2: Comparative analytical data for the detection of DEAET and hydrazine at chemically modified electrodes.

Electrodes	**Methods**	**Analytical Parameters**			
		LCR / μM	**LoD/ μM**	***Sensitivity*** **/μAμM^{-1}**	**Ref**
	DEAET				
SPE- MWCNT-OPH	CA	50-250	8.0	36.0	22
GCE-PPy-PQQ	CA	5.8-100	3.0	0.00137 cm^{-2}	24
BPPGE-SWCNT-CoTAPc	CA	-	3.0	0.06	16
BPPGE-Ni powder	CA	0.01-100	4.0	0.023	4
BPPGE-MWCNT-Ni	CA	91.0-333.0	0.87±0.07	13.6±0.33cm^{-2}	This work
	Hydrazine				
Pd-BDD array Pd-Macroelectrode	LSV	6.8-102 30.6-204	1.8 2.6	0.008 0.06	26
CM-MWCNT-GCE	CA	2.0 – 44	1.4	0.0229	19
CCE-NiHCF	CV	20 - 2000	8.0	-	25
IMWCNTCPE	DPV	0.6-8.0 8.0-100.0	0.29	0.167 0.014	26
ST-NiTsPc	CA	100-600	10	–	27
BPPGE-MWCNT-Ni	CA	91.0-333.0	0.29±0.02	3.33±0.13cm^{-2}	This work

Chronoamperometry; LSV: Linear sweep voltammetry; DPV: Differential pulse voltammetry; SPE- MWCNT-OPH: Screen-printed carbon electrode modified with multi-walled carbon nanotubes and organophosphorus hydrolase; GCE-PPy-PQQ: Glassy carbon electrode modified with poplypyrrole and pyrroloquinoline quionone; BPPGE-SWCNT-CoTAPc: Basal plane pyrolytic graphite electrode modified with single-walled carbon nanotube and cobalt tetraaminophthalocyanine; BPPGE-Ni powder: Basal plane pyrolytic graphite electrode modified with nickel micropowders;Pd-BDD: palladium modified with boron-doped diamond microelectrode array; CM-MWCNT-GCE:Curcumin- multi-walled carbon nanotube modified glassy carbon electrode; CCE-NiHCF: carbon ceramic electrode (CCE) modified with nickel hexacyanoferrate; IMWCNTCCE: indenedione derivatives multi-walled carbon nanotube modified carbon ceramic electrode; ST-NiTsPc: Nickel tetrasulfonated phthalocyanine (NiTsPc) immobilized onto titanized silica gel.

Based on the report of hydrazine oxidation in aqueous medium [29], the following general mechanism for the oxidation of the analyte on the EPPGE-MWCNT-Ni electrode is suggested:

$$[\text{MWCNT-Ni}^{2+}]_{\text{film}} \longrightarrow [\text{MWCNT-Ni}^{3+}]_{\text{film(aq)}} + e^- \quad (5.9)$$

$$[\text{MWCNT-Ni}^{3+}]_{\text{film(aq)}} + N_2H_{4(aq)} \rightleftharpoons [\text{MWCNT-Ni}^{3+}\text{----}N_2H_{4(aq)}]_{\text{adduct}} \quad (5.10)$$

$$[\text{MWCNT-Ni}^{3+}\text{----}N_2H_{4(aq)}]_{\text{adduct}} \rightleftharpoons [\text{MWCNT-Ni}^{2+}]_{\text{film}} + N_2H_{3(aq)} + e^- \quad (5.11)$$

slow (rate limiting)

$$N_2H_3 + 3H_2O \longrightarrow N_2 + 3H_3O^+ + 3e^- \quad (5.12)$$

$$[\text{MWCNT-Ni}^{3+}]_{\text{film(aq)}} + e^- \longrightarrow [\text{MWCNT-Ni}^{2+}]_{\text{film}} \quad (5.13)$$

$$N_2H_4 + 4H_2O \longrightarrow N_2 + 4H_3O^+ + 4e^- \quad \text{(Overall reaction)} \quad (5.14)$$

Equation 5.9 defines the redox process of the nickel species confined in the MWCNT. The interaction of the Ni^{3+} with aqueous hydrazine results to the formation of an adduct (Equation 5.10). The adduct undergoes an internal reaction leading to the formation of hydrazine oxidation intermediate (N_2H_3) and the generation of Ni^{2+} (Equation 5.11). This also represents the rate-determining step, a one-electron process. Equation 5.12 represents the oxidation of the intermediate to give nitrogen as the final product, while Equation 5.13 represents the regeneration of the original nickel (II) catalyst. The overall electrocatalytic oxidation reaction of hydrazine (Equation 5.14) is thus a 4-electron process as also proposed by others [14, 30].

For DEAET, the mechanism follows a similar process, summarised as follows:

$$RSH + OH^- \rightleftharpoons RS^{\cdot} + H_2O \quad (5.15)$$

$$[MWCNT\text{-}Ni^{3+}]_{film(aq)} \; RS^- \rightleftharpoons [MWCNT\text{-}Ni^{3+}\text{----}(RS)]_{adduct} \quad (5.16)$$

$$[MWCNT\text{-}Ni^{3+}\text{----}(RS)]_{adduct} \rightleftharpoons [MWCNT\text{-}Ni^{2+}]_{film} \; RS^{\cdot} + e^- \quad (5.17)$$

slow (rate limiting)

$$RS^{\cdot} + RS^{\cdot} \longrightarrow RSSR \quad (fast) \quad (5.18)$$

The DEAET represented as a thiol (RSH) forms a thiyl ion (RS^-) in basic medium (Equation 5.15). The MWCNT-Ni^{2+} film interact with the thiyl ion (RS^-) in solution forming an adduct (Equation 5.16). The adduct rearranged to give the thiyl radical in a one-electron process which represent the rate-determining step (Equation 5.17). The thiyl radical ($RS^{\bullet}$) then dimerises to form the disulphide product (Equation 5.18). As in the hydrazine mechanism, Equations 5.9 and 5.13 still hold.

This study has shown that the MWCNT-Ni nanocomposite modified electrode yielded the fastest electron transport as well as the best electrocatalytic behaviour towards DEAET and hydrazine compared with other electrodes investigated or reported in the literature. This enhancement is associated with high electrical-conducting MWCNTs which form a synergistic behaviour with nickel nanoparticles. Electrocatalysis of DEAET on the EPPGE-MWCNT-Ni was predominantly diffusion-controlled, with little or no adsorption of reaction intermediates. The adsorption equilibrium constant (β) and the Gibbs free energy change due to adsorption ΔG^o for the EPPGE-MWCNT-Ni electrode in DEAET and hydrazine were estimated as 1.51×10^3 M^{-1} (-18.14 $kJmol^{-1}$) and 1.04×10^3 M^{-1} (– 17.21 $kJmol^{-1}$), respectively.

References

1. S.H. Wu, D.H. Chen, *J. Colloid Interf. Sci*. 259 (2003) 282.

2. L. Xiang, X.Y. Deng, Y. Jin, *Scripta Materialia* 47 (2002) 219.

3. D. Nkosi, J. Pillay, K. I. Ozoemena, K. Nouneh and M. Oyama, *Phys. Chem. Chem. Phys*. 12 (2010) 604.

4. J. Pillay, K.I. Ozoemena, *Electrochem. Commun.* 9 (2007) 1816.

5. L. Yang, Y. Li, *Biosens. Bioelectron*. 20 (2005) 1407.

6. K.I. Ozoemena, T. Nyokong, *Inorg. Chem. Commun.* 6 (2003) 1192.

7. J. Bisquert, H. Randriamahazaka, G. Garcia-Belmonte, *Electrochim Acta* 51(2005) 627.

8. M. Jafarian, M.G. Mahjani, H. Heli, F. Gobal, H. Khajehsharifi, M.H. Hamedi *Electrochim Acta* 48 (2003) 3423.

9. S. Majdi, A. Jabbari, H. Heli, A.A. Moosavi-Movahedi *Electrochim Acta* 52 (2007) 4622.

10. W-H Su, S-H Cheng, *Electrochem. Commun*. 10 (2008) 899-902.

11. Y.-C. Yang, L.L. Szafraniec, W.T. Beaudry, D.K. Rohrbaugh, L.R. Procell, J.B. Samuel, *J. Org. Chem.* 61 (1996) 8407.

12. A.J. Bard, L.R. Faulkner, Electrochemical Methods: Fundamentals and Applications, 2nd ed., John Wiley & Sons, Hoboken, N.J., 2001.

13. A-G Boudjahem, S. Monteverdi, M. Mercy, and M.M. Bettahar, *Langmuir* 20 (2004) 208.

14. J.A. Harison, Z.A. Khan, *J. Electroanal. Chem.* 28 (1970) 131.

15. J.N. Soderberg, A.C. Co, A.H.C Sirk, V.I. Birss, *J. Phys. Chem. B* 110 (2006) 10401.

16. J. Pillay, K.I. Ozoemena, *Electrochim. Acta* 52 (2007) 3630.
17. J. Li, X.Q. Lin, *Sens. Actuat. B: Chem.* 126 (2007) 527.

18. H. M. Nassef, A.-E. Radi, C. K. O'Sullivan, *J. Electroanal. Chem.* 592 (2006) 139.

19. L. Zheng, J.-f. Song, *Sens. Actuators B* 135 (2009) 650.

20. Q. Yi, W. Yu, J. *Electroanal. Chem.* 633 (2009) 159.

21. G. D. Christian, 2004 Analytical Chemistry, 6th ed. John Wiley and Sons New York, p 113.

22. K. A. Joshi, M. Prouza, M. Kum, J. Wang, J. Tang, R. Haddon, W. Chen, A. Mulchandani, *Anal. Chem.* 78 (2006) 331.

23. J. Wang, J. Zima, N.S. Lawrence, M.P. Chatrathi, *Anal. Chem.* 76 (2004) 4721.

24. O.V. Shulga, C. Palmer, *Anal. Bioanal. Chem*. 385 (2006) 1116.

25. A. Abbaspour, A. Khajehzadeh, A. Ghaffarinejad, *J. Electroanal. Chem.* 631 (2009) 52.

26. H.R. Zare, N. Nasirizadeh, F. Chatraei, S. Makarem, *Electrochim. Acta* 54 (2009) 2828.

27. E.F. Perez, G.-O. Neto, A.A. Tanaka, L.T. Kubota, *Electroanalysis* 10 (1998) 111.

28. H.X. Ju, L. Donal, *J. Electroanal. Chem*. 48 (2000) 150.

29. A. Abbaspour, M. Shamsipur, A. Sironeinejad, R. Kia, P.R. Raithby, *Electrochim. Acta* 54 (2009) 2916.

30. C. batchelor-McAuley, C.E. Banks, A.O. Simm, T.G.J. Jones, and R.G. Compton, *Analyst* 131 (2006) 106.